Dyes and Pigments 80 (2009) 174–180

Contents lists available at ScienceDirect

Dyes and Pigments

journal homepage: www.elsevier.com/locate/dyepig

The synthesis, photophysical properties and two-photon absorption of triphenylamine multipolar chromophores

Ying Qian [a,*], Kang Meng [a], Chang-Gui Lu [b], Bao-ping Lin [a], Wei Huang [b], Yi-Ping Cui [b]

[a] School of Chemistry and Chemical Engineering, Southeast University, Nanjing 211189, China
[b] School of Electronic Science and Engineering, Southeast University, Nanjing 210096, China

ARTICLE INFO

Article history:
Received 21 March 2008
Received in revised form 6 July 2008
Accepted 7 July 2008
Available online 18 July 2008

Keywords:
Triphenylamine derivatives
Multipolar chromophore
Two-photon absorption
Two-photon excited fluorescence
Optical power limiting
Solvatochromic behavior

ABSTRACT

Triphenylamine core multipolar derivatives were synthesized via the Wittig reaction and Heck reaction and were characterized by MS, NMR, IR; melting points and decomposition temperatures were determined using differential scanning calorimetry. The photophysical as well as the linear and nonlinear spectral properties of multipolar compounds with a triphenylamine core were compared to those of corresponding dipolar compounds. The multipolar chromophores displayed large two-photon absorption and strong optical power limiting properties. An extended π-conjugated system and increased intramolecular cooperative effect are responsible for the observed, large two-photon absorption character.

1. Introduction

Molecular dendrimers constitute a new class of organic nanostructures with multipolar geometry. The dendrimers constructed from optically active blocks show intriguing two-photon absorption (TPA) properties which have wide range of applications such as optical power limiting, high-resolution three-dimensional imaging of biological systems, laser upconversion and two-photon photodynamic therapy, microfabrication, or three-dimensional optical data storage [1–5]. Depending on the applications, two-photon chromophores have to satisfy different kinds of requirements. For instance, the combination of high fluorescence quantum yield and TPA cross-section in the red-NIR range is desirable for biological imaging. In recent years, considerable effort has been devoted to the design and investigation of two-photon chromophores, exploring in particular the multipolar strategy. A major advantage of the multipolar structure originates from the intramolecular coupling and cooperative enhancement of TPA. This enhancement is correlated to intramolecular interactions that occur between the branches and the center of the molecules. Increasing the extent of charge transfer from the ends to the middle results in a large increase of two-photon absorption [6–11].

We have designed and synthesized a specific class of substituted stilbene chromophores, which comprises triphenylamine as a core and an electron-withdrawing group 3,5-di-{5-[4-(*tert*-butyl)-phenyl]-1,3,4-oxadiazol-2-yl}-styrene as conjugated arms (see Fig. 1). The grafting of one, two, or three branches on an electron-donating trigonal moiety triphenylamine leads to multipolar chromophores of different symmetry: dipolar, V-shaped, and octupolar. Compared to one-dimensional molecules, multipolar chromophores have appeared to show promising properties. It is expected that the electronic push–pull structures in the arm and their cooperative effect help the extended charge transfer for TPA. A butyl moiety is attached to the end of each arm to induce the optical transparency as well as the good solubility to various organic solvents.

In this paper, we describe the synthesis and characterization of novel multipolar chromophores. Linear absorption and fluorescence properties of chromophores, as well as the solvatochromic behavior of one-photon spectra are then thoroughly explored through experimental results. In particular, we have investigated the effect of branching of dipolar chromophores on photoluminescence and TPA including UV–visible, fluorescence, TPA coefficient and two-photon excited fluorescence (TPEF) measurements.

2. Experimental

2.1. Materials

Triphenylamine, palladium(II) diacetate, tris-*o*-tolylphosphine, potassium *tert*-butoxide, and phosphorus oxychloride were

* Corresponding author. Fax: +86 25 84038250.
E-mail address: yingqian@seu.edu.cn (Y. Qian).

0143-7208/$ – see front matter © 2008 Elsevier Ltd. All rights reserved.
doi:10.1016/j.dyepig.2008.07.005

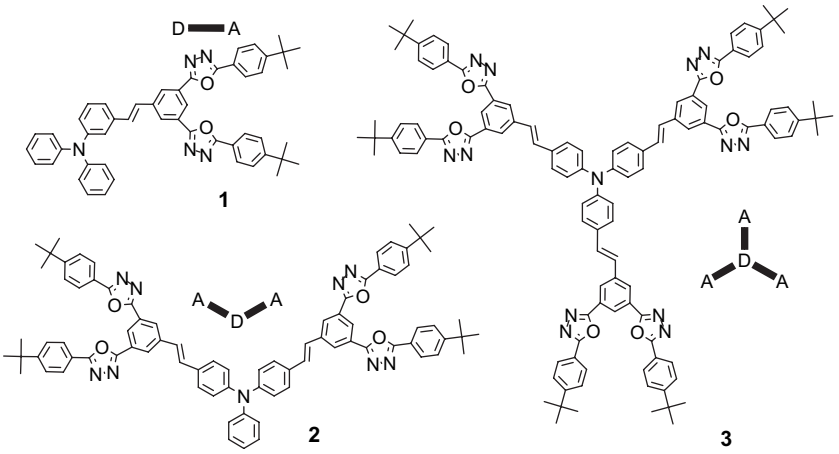

Fig. 1. Series of structurally related dipolar chromophore (**1**), V-shaped chromophore (**2**), and octupolar chromophore (**3**) derived from the functionalization of a triphenylamine moiety.

purchased from Aldrich Chemical Co. All solvents were of anhydrous grade after further purification. 4-(Diphenylamino)-benzaldehyde, bis(4-formylphenyl)phenylamine, and tris(4-bromophenyl)amine were prepared from triphenylamine using a previously reported procedure [12,13]. All other chemical reagents were obtained commercially and were used as received without further purification.

The synthesis of electron-withdrawing functionalized oxadiazole compound was accomplished by straightforward series of reactions. As shown in Fig. 2, before the formation of heterocyclic oxadiazole ring, the coupling reaction between 5-methyl-1,3-benzoyl dichloride and 4-*tert*-butyl benzoyl hydrazine should be accomplished. Simple ring formation by condensation of water from amide compound in the presence of $POCl_3$ gave rise to compound M_4. Free radical bromination of M_1 was set-up to afford bromomethyl compound M_3 and to be transformed into phosphonium bromide salt M_2. Finally, this Wittig precursor, M_2 was reacted with formaldehyde to give compound 3,5-di-{5-[4-(*tert*-butyl)phenyl]-1,3,4-oxadiazol-2-yl}-styrene (M_1). Yield 83%; IR (cm^{-1}): 2962, 2871 (–CH_3), 1614 (C═C), 1570, 1492 (–Ph), 910, 995 (–CH═CH_2); ^1H NMR (300 MHz, $CDCl_3$): δ 1.40 (s, 18H, –CH_3), 5.57 (d, 1H, $J = 10.92$, ═CH_2), 6.09 (d, 1H, $J = 17.58$, ═CH_2), 6.88–6.93 (m, 1H, –CH═), 7.61 (d, 4H, $J = 8.55$), 8.15 (d, 4H, $J = 8.55$), 8.36 (s, 2H), 8.73 (s, 1H); MS (*m*/*z*): 505.3 $[M + H]^+$,544.5 $[M + K]^+$.

2.1.1. N-*[4-{2-(3,5-Di-{5-[4-(*tert*-butyl)phenyl]-1,3,4-oxadiazol-2-yl}phenyl)-1-ethenyl}phenyl]*-N,N-*diphenylamine (chromophore **1**)*

To a solution of 4-(diphenylamino)benzaldehyde (1.00 g, 3.66 mmol) and M_2 (3.05 g, 3.66 mmol) in CH_2Cl_2 was added *t*-BuOK (1.22 g, 10.98 mmol). The mixture was stirred for 24 h, and the solvent was removed under reduced pressure. After the addition of water, extraction with CH_2Cl_2, and drying with Na_2SO_4, the solvent was evaporated. The crude product was purified by column chromatography (petroleum ether/ethyl acetate, 6:1) to afford chromophore **1**. Yield 68%; IR (cm^{-1}): 2962, 2869 (–CH_3), 1616 (C═C), 1592, 1460 (–Ph), 965 (*trans*-CH═CH–); ^1H NMR (300 MHz, $CDCl_3$): δ 1.40 (s, 18H), 6.91 (d, 2H, $J = 17.20$ Hz), 7.08–7.11 (m, 5H), 7.14–7.16 (m, 5H), 7.46 (d, 4H, $J = 8.55$ Hz), 7.59 (d, 4H, $J = 8.58$ Hz), 8.13 (d, 4H, $J = 8.55$ Hz), 8.44 (s, 2H), 8.68 (s, 1H); FAB-MS (*m*/*z*): 747.5 $[M]^+$, 748.5 $[M + H]^+$.

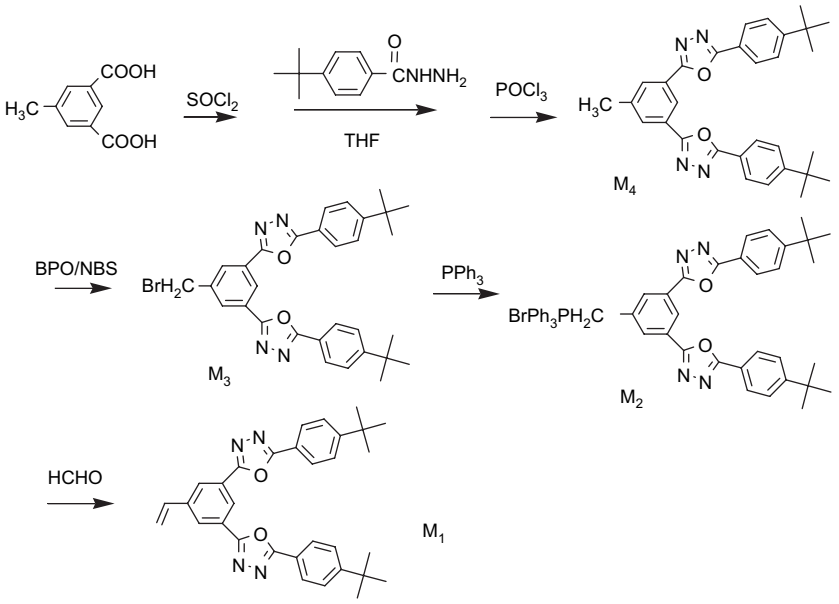

Fig. 2. Synthetic routes of compound M_1.

2.1.2. N,N-*Bis[4-{2-(3,5-di-{5-[4-*(tert-*butyl)phenyl]-1,3,4-oxadiazol-2-yl}phenyl)-1-ethenyl}phenyl]*-N-*phenylamine (chromophore **2**)*

Chromophore **2** was prepared by the same procedure as described for **1** using the mixture of bis(4-formylphenyl)phenylamine and M_2 in CH_2Cl_2. Purification was carried out by chromatography on a silica gel column. Yield 45%; IR (cm^{-1}): 2971, 2870 (–CH_3), 1618 (C═C), 1591, 1450 (–Ph), 965 (*trans*-CH═CH–); ^{1}H NMR (300 MHz, $CDCl_3$): δ 1.40 (s, 36H), 5.31 (s, 4H), 7.11–7.19 (m, 5H), 7.51 (d, 8H, $J = 8.52$ Hz), 7.59 (d, 8H, $J = 8.43$ Hz), 8.13 (d, 8H, $J = 8.46$ Hz); FAB-MS (*m*/*z*): 1249.2 $[M]^+$, 1250.0 $[M + H]^+$.

2.1.3. N,N,N-*Tris[4-{2-(3,5-di-{5-[4-(*tert-*butyl)phenyl]-1,3,4-oxadiazol-2-yl}phenyl)-1-ethenyl}phenyl] amine (chromophore **3**)*

A mixture of tris(4-bromophenyl)amine (0.30 g, 0.60 mmol) and M_1 (12.10 g, 2.40 mmol), palladium(II) diacetate (0.0066 g, 0.03 mmol), tris-*o*-tolylphosphine(0.019 g, 0.06 mmol), and 3.5 mL of triethylamine in 6.5 mL of DMF was stirred at room temperature for 1 h with N_2 bubbling. And then the mixture was stirred at 110 °C for 96 h in a N_2 atmosphere. After cooling, it was poured into 50 mL of methanol. The precipitate was filtered and dried after repeatedly washing with methanol. Purification was carried out by chromatography on a silica gel column (petroleum ether/ethyl acetate, from 6:1 to 2:1) to afford chromophore **3**. Yield 43%; IR (cm^{-1}): 2962, 2870 (–CH_3), 1621 (C═C), 1592, 1510 (–Ph), 968 (*trans*-CH═CH–); ^{1}H NMR (300 MH_Z, $CDCl_3$): δ 1.40 (s, 54H, –CH_3), 7.09 (d, 2H, $J = 11.94$ Hz, –CH═CH–), 7.17 (d, 2H, $J = 11.86$ Hz, –CH═CH–), 7.25 (d, 2H, $J = 12.75$ Hz, –CH═CH–), 7.40–7.56 (m, 8H, Ph–H), 7.62 (d, 16H, $J = 8.52$ Hz, Ph–H), 8.17 (d, 12H, $J = 8.19$, Ph–H), 8.46–8.48 (m, 6H, Ph–H), 8.70 (s, 3H, Ph–H); FAB-MS (*m*/*z*): 1751.0 (M^+), 1752.0 $[M + H]^+$.

2.2. Methods

All the optical characterizations were conducted using solutions of compounds in dichloromethane. UV–visible absorption was conducted using a Shimadzu UV-3600 spectrophotometer, single-photon fluorescence was conducted using a Edinbough FLS920 spectrofluorophotometer. ^{1}H NMR spectra were measured on a Bruker 300 MHz apparatus using $CDCl_3$ as solvent. FTIR spectra were recorded on a Nicolet 750 series in the region of 4000–400 cm^{-1} using KBr pellets. MS spectra were measured on a TSQ Quantum Ultra Workstation.

Two-photon absorption cross-section values of all the chromophores in solution were investigated by a direct nonlinear transmission (NLT) method with nanosecond pulse [14,15]. This method involves the measurement and study of the relation between optical input and output intensities. Basically, a linearly polarized 800 nm pulsed laser beam is used as the testing beam, which is provided by a dye laser system pumped with a frequency-doubled and Q-switched Nd:YAG laser. This laser beam is focused and passed through a quartz cuvette filled with the sample solution and the transmitted laser beam from the sample cell can be detected by an optical power meter. Thus, if the tested sample does not have a linear absorption at 800 nm, only the transmissivity change due to pure nonlinear absorption could be measured. The experimental set-up and data processing procedure are basically the same as those described in the previous publications.

3. Results and discussion

3.1. Synthesis and characterization

We have synthesized a specific class of substituted stilbene chromophores, which comprises triphenylamine as an electron-donating trigonal core and an electron-withdrawing group 3,5-di-{5-[4-(*tert*-butyl)phenyl]-1,3,4-oxadiazol-2-yl}-styrene as conjugated arms. The synthetic routes to these chromophores are described in Figs. 2 and 3. All the chromophores were obtained after carefully purified by column chromatography and confirmed by ^{1}H NMR, MS, and IR. The data were found to be in good agreement with the proposed structures. The chromophores **1**–**3** after thorough purification were highly soluble in many organic solvents, such as dichloromethane, chloroform, THF, ethyl acetate, and DMF at room temperature.

Chromophore **3** was prepared from the vinyloxadiazole compound M_1 and tris(4-bromophenyl)amine under palladium-catalyzed Heck coupling reaction with 43% yield. Nucleophilic attack of olefins of palladium(II) thus produced first C–Pd–C bonds which rearranged to form C–C bonds. Chromophores **1** and **2** were

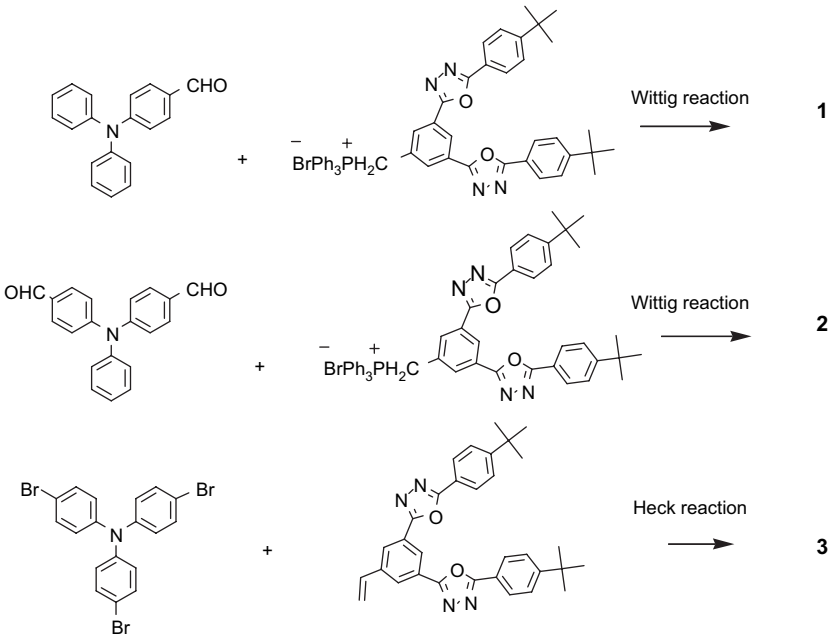

Fig. 3. Synthesis of target chromophores **1**–**3**.

synthesized by Wittig reaction of formylated triphenylamine core with phosphorus ylid derivatives. Wittig reaction is an important synthetic route for the formation of olefin functional group. In general, Wittig reaction involves the coupling between an aldehyde and a phosphorus ylid to produce carbon–carbon double bond. Formylated triphenylamine and benzylphosphonium bromide salt are used as the reactants in Fig. 3. It is noteworthy that in our case, the major product of Wittig reaction is the *trans* form of the stilbenoid compounds. IR absorption corresponding to *trans* double bond of compounds **1**–**3** is in the range of 965–968 cm^{-1}.

The behaviour of chromophores **1**–**3** upon heating was determined by DSC and TGA under a nitrogen atmosphere (Fig. 4). The samples were heated in a pan at the rate of 10 °C/min to give the melting point (T_m) and the decomposition temperature (T_d) listed in Table 1. The temperatures at 5% and 10% weight loss (T_{d5}, T_{d10}) of the chromophores are summarized in Table 1. Chromophores **1**–**3** show decomposition temperature between 373 and 412 °C, and relatively higher thermal stability. The six-branched chromophore **3** exhibited a slightly higher temperature of thermal decomposition compared with that of four- and two-branched chromophores.

The electrochemical properties of multibranched chromophores determined by cyclic voltammetry are reported in Table 1 and Fig. 5. The ionization potential (I_p) and electron affinity (E_a) of chromophores were estimated by using the following relations: $[E_{onset}]_{ox} = I_p - 4.46$ and $E_a = I_p - E_g$, where $[E_{onset}]_{ox}$ are the onset potentials for the oxidation of chromophores versus saturated calomel electrode (SCE). The band gap energy (E_g) was determined from the onset point of the absorption spectrum.

3.2. Photophysical properties of chromophores

The fundamental building block molecule M_1 can be considered as a repeating unit for chromophores **1**–**3**. These multiarmed derivatives involve linkage of one, two, and three M_1 units through the center electron-donating trigonal moiety triphenylamine. The absorption spectra of chromophores **1**–**3** are shown in Table 2. All chromophores show good transparency in a wide range of the visible region and intense absorption in the near-UV–visible region (Table 2). The absorption band at about 300 nm is assigned to absorption of the phenylene ring, whereas the longer wavelength region absorption band is attributed to a charge-transfer band of the molecules. A bathochromic shift is observed with increasing conjugated arms. The maximum peaks of linear absorption corresponding to the charge-transfer bands are at 390 nm for the single branched compound **1**, at 398 nm for the bis-branched compound **2**, and at 408 nm for the tri-branched compound **3** in CH_2Cl_2, respectively. The maximum absorption of compound M_1 is observed at 295 nm.

Table 1
Thermal degradation temperature and electrochemical properties of chromophores **1**–**3**

No.	T_m (°C)	T_{d5} (°C)	T_{d10} (°C)	T_d (°C)	I_p (eV)	E_a (eV)	E_g (eV)
1	156	171	297	373	5.18	2.32	2.86
2	197	187	331	412	5.15	2.37	2.78
3	208	250	375	398	5.14	2.41	2.73
M_1	144	253	358	392	–	–	–

Chromophores **1**–**3** fluoresce blue in the solid state under conventional laboratory UV-lampusing 400 nm excitation wavelength in CH_2Cl_2 at a concentration of 10^{-5} mol/L. Table 2 shows that the single-photon excited fluorescence of **1** is in the blue region with a peak at 486 nm. Chromophore **2** exhibits an emission in the blue region with a peak at 483 nm. Chromophore **3** exhibits a strong emission in the blue region with a peak at 487 nm. The emission of branched compound M_1 is observed at 360 nm.

Possible solvent influence on the linear absorption and fluorescence behavior is investigated. The absorption and fluorescence spectra of **1**–**3** in four different solvents, ethyl acetate, THF, CH_2Cl_2, DMF, at a concentration of 10^{-5} M are shown in Table 2. The absorption and emission maxima and shapes of chromophores **1**–**3** exhibit solvent polarity dependencies. All three chromophores show a marked positive emission solvatochromism: increasing solvent polarity leads to a pronounced bathochromic shift of the emission band. In contrast, no noticeable shift is observed for the absorption band. Accordingly, the Stokes shifts significantly increase with increasing solvent polarity. As shown in Table 2, the solvatochromic behavior of dipolar chromophores can be fitted with a Lippert–Mataga relationship, given in Eq. (1) [16,17]:

$$\tilde{\nu}_{abs} - \tilde{\nu}_{em} = \frac{2\left(\mu_{ee}^{f} - \mu_{gg}\right)^2 \Delta f}{hca^3} + \text{const} \quad (1)$$

$$\Delta f = \frac{\varepsilon - 1}{2\varepsilon + 1} - \frac{n^2 - 1}{2n^2 + 1} \quad (2)$$

where $\tilde{\nu}_{abs}$ is the wavenumber of the absorption maximum, $\tilde{\nu}_{em}$ is the wavenumber of the fluorescence maximum, h is the Planck

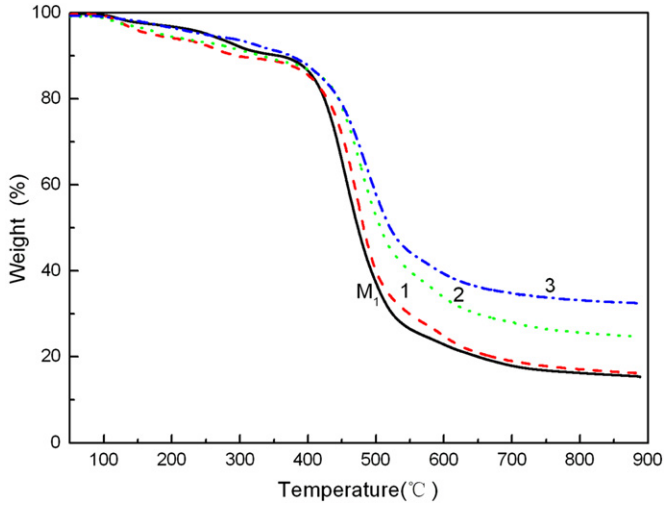

Fig. 4. TGA thermograms of chromophores **1**–**3**.

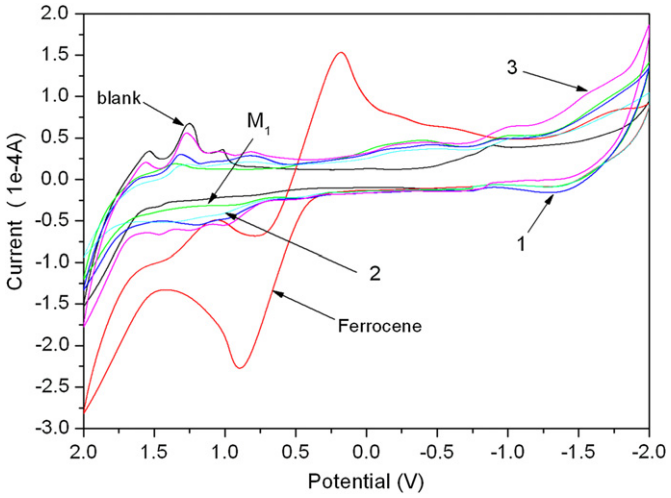

Fig. 5. Cyclic voltammograms of chromophores in CH_2Cl_2 at 50 mV/s scan rate.

Table 2
Photophysical properties of chromophores **1–3**

No.	λ_{abs} (nm)[a]	$\lambda_{cut\text{-}off}$ (nm)[b]	ε (10^3 M^{-1} cm^{-1})	λ_{em} (nm)[c]	Stokes shift[d] (10^3 cm^{-1})	Slope (10^3 cm^{-1})	Φ[e]
1	390(1)	434	4.56	486(1)	5.07(1)	24.3	0.78
	380(2)			470(2)	5.04(2)		
	387(3)			474(3)	4.74(3)		
	381(4)			517(4)	6.09(4)		
2	398(1)	446	6.97	483(1)	4.42(1)	27.8	0.80
	391(2)			473(2)	4.43(2)		
	400(3)			477(3)	4.04(3)		
	387(4)			520(4)	6.61(4)		
3	408(1)	452	11.66	487(1)	3.98(1)	36.8	0.79
	400(2)			476(2)	3.99(2)		
	407(3)			479(3)	3.69(3)		
	405(4)			521(4)	5.50(4)		

[a] Absorption maximum in CH_2Cl_2(1) ,ethyl acetate(2), THF(3), DMF(4).
[b] Wavelength at which the transmittance is 95%, in CH_2Cl_2.
[c] Emission maximum in CH_2Cl_2(1) ,ethyl acetate(2), THF(3), DMF(4).
[d] Stokes shift $= (1/\lambda_{abs} - 1/\lambda_{em})$ in CH_2Cl_2(1) ,ethyl acetate(2), THF(3), DMF(4).
[e] Fluorescence quantum yield in CH_2Cl_2.

constant, c is the light velocity, a is the radius of the solute spherical cavity, ε is the dielectric constant and n is refractive index of the solvent. In the simple case where the dipole moment of the vertical (Franck–Condon) excited state (created immediately after absorption) and the dipole moment of the relaxed excited states are identical (as are vertical and relaxed ground-state dipoles), $\Delta\mu_{eff}$ corresponds to excited-state dipole moment μ_{ee} and ground-state dipole moment μ_{gg}.

Solvatochromic slopes derived from the Lippert–Mataga fit of the experimental Stokes shift are reported in Table 2. Table 2 clearly shows that Stokes shift actually follows the trend predicted by Eq. (1). Thus, we believe that the Lippert–Mataga relationship qualitatively describes our data. The Lippert–Mataga slopes for the three-branch octupoles is larger than those of their dipolar counterparts. Increasing solvent polarity induces a slight red-shift of the absorption band and a marked bathochromic shift of the emission band. In the case of dipolar systems, such behavior is typical of an ICT transition with an increase of dipole moment upon excitation and the emission is delocalized on triphenylamine-based multibranched structures.

Fluorescence quantum yield in CH_2Cl_2 was determined using quinine in 0.5 N H_2SO_4 as a standard. The fluorescence quantum yield of branch molecule M_1 is 0.34. The multibranched derivatives involve linkage of one, two, and three M_1 units through the center moiety triphenylamine reach to high fluorescence quantum yield (0.78–0.80), which a number of factors are electronic delocalization and intramolecular charge-transfer phenomena.

3.3. Two-photon absorption of chromophores

We obtained the effective molecular TPA coefficient of chromophores **1–3** at a concentration of 1.0×10^{-2} mol L^{-1} in dichloromethane and DMF. Two-photon excited fluorescence spectra measured are shown in Fig. 6(a) and (b). Fig. 7 shows normalized UV–visible absorption and one-photon excited fluorescence, and two-photon excited fluorescence of TPA chromophores **1–3** in CH_2Cl_2. The one-photon fluorescence excitation wavelength is 400 nm and the two-photon fluorescence is excited by a Q-switched and frequency-doubled Nd:YAG laser at 800 nm. The maximum peaks of one-photon and two-photon fluorescence are at 486 and 502 nm for chromophore **1** and at 483 and 515 nm for chromophore **2**, and at 487 and 518 nm for chromophore **3** in dichloromethane. In comparison with the corresponding one-photon fluorescence, the red-shift for two-photon fluorescence is obtained because of their different excitation modes.

Fig. 8 shows the optical power limiting measured by the NLT method with nanosecond pulse. It is seen that the intensity of the transmitted laser beam increased nonlinearity as that of the incident laser beam. The nonlinear absorption coefficient was obtained by fitting the experimental data given in Eq. (4) [18]:

$$T(I_0) = \frac{I(L)}{I_0} = \frac{1}{1 + I_0 L\beta} \tag{3}$$

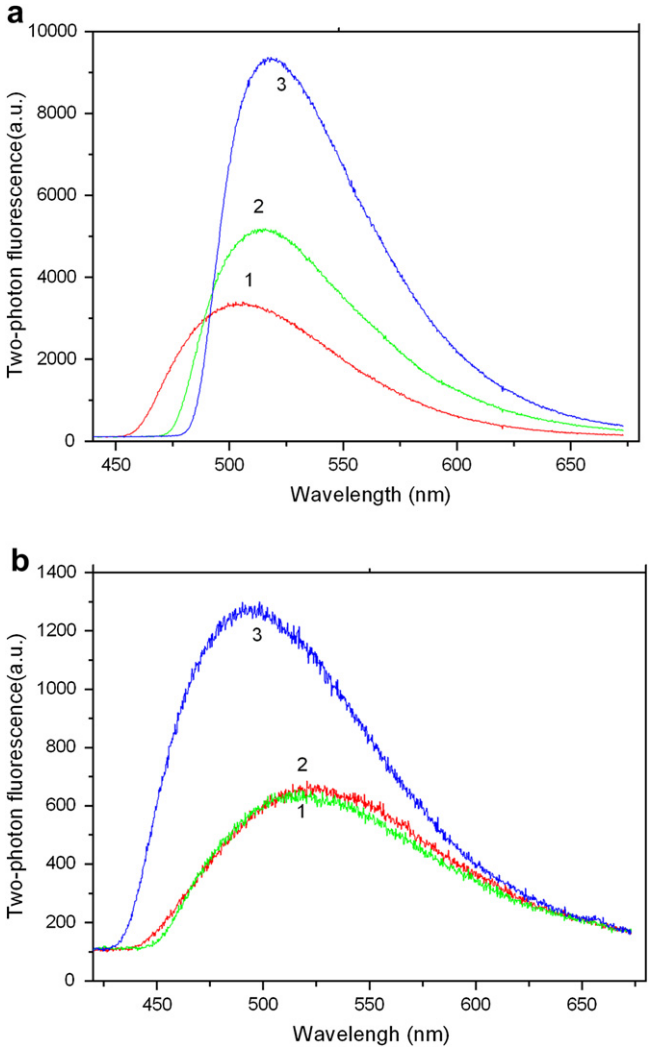

Fig. 6. Two-photon excited fluorescence (TPEF) of **1–3** in CH_2Cl_2 (a) and DMF (b).

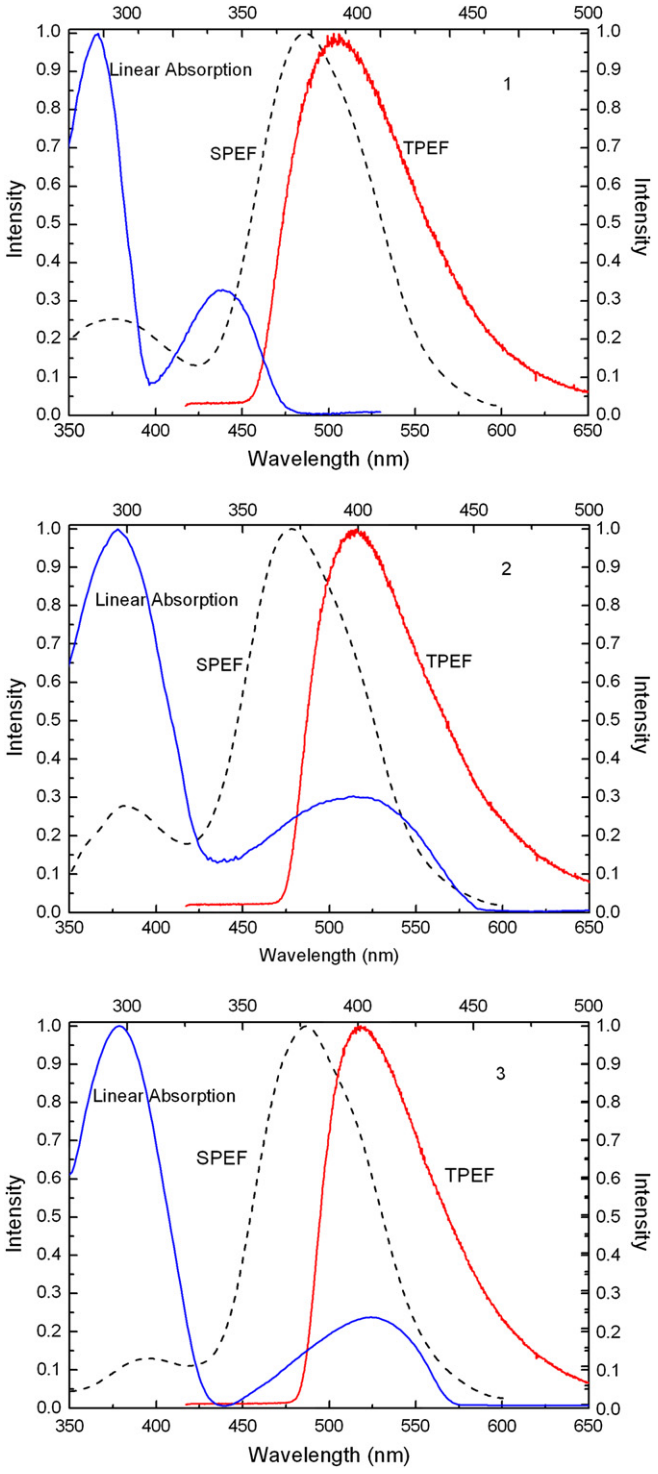

Fig. 7. Normalized UV absorption and one-photon excited fluorescence, and two-photon excited fluorescence of TPA chromophores **1**–**3** in CH_2Cl_2.

where I_0 is the incident intensity, L is the thickness of the solution sample, and β is the TPA coefficient of the solution. The TPA coefficient β (in units of cm/GW) of a given solution sample is determined by

$$\beta = \frac{\sigma_2 N_0}{h\nu} = \frac{\sigma_2 N_A d \times 10^{-3}}{h\nu} \tag{4}$$

where N_0 is the molecular density of the chromophore, σ_2 is the molecular TPA cross-section (in units of cm^4 s), d is the concentration of the TPA chromophore in (in units of mol/L), N_A is the Avogadro constant, $h\nu$ is the energy of the incident photon. TPA is the dominant mechanism causing the observed nonlinear absorption behavior. However, as many researchers have indicated the strong TPA process considerably increases molecular population in the excited state, which, in turn, creates an additional contribution to the observed nonlinear absorption of the input laser beam. The TPA cross-section is used as a parameter to compare the relative magnitude of TPA-dominated nonlinear absorptivity. Because it was not possible to separate pure TPA from EAS contribution through the ns NLT measurement, the term "effective TPA coefficient" is used to describe the TPA values for the chromophores in the paper.

$$\beta \propto \mu_{ge}^2 \left(\mu_{ee} - \mu_{gg}\right)^2 \tag{5}$$

The effective TPA coefficient β is proportional to the product of the square of the transition dipole moment and the square of the difference between excited-state and ground-state dipole moments [13], given in Eq. (5). Data in Table 3 suggest that there is increase in β of chromophores **3** and **2** with respect to chromophore **1**. This is confirmed by the more pronounced solvatochromic behavior as described by the slope values. Indeed, while the solvatochromic slope is proportional to $\Delta\mu_{eff}^2$ and the TPA coefficient to

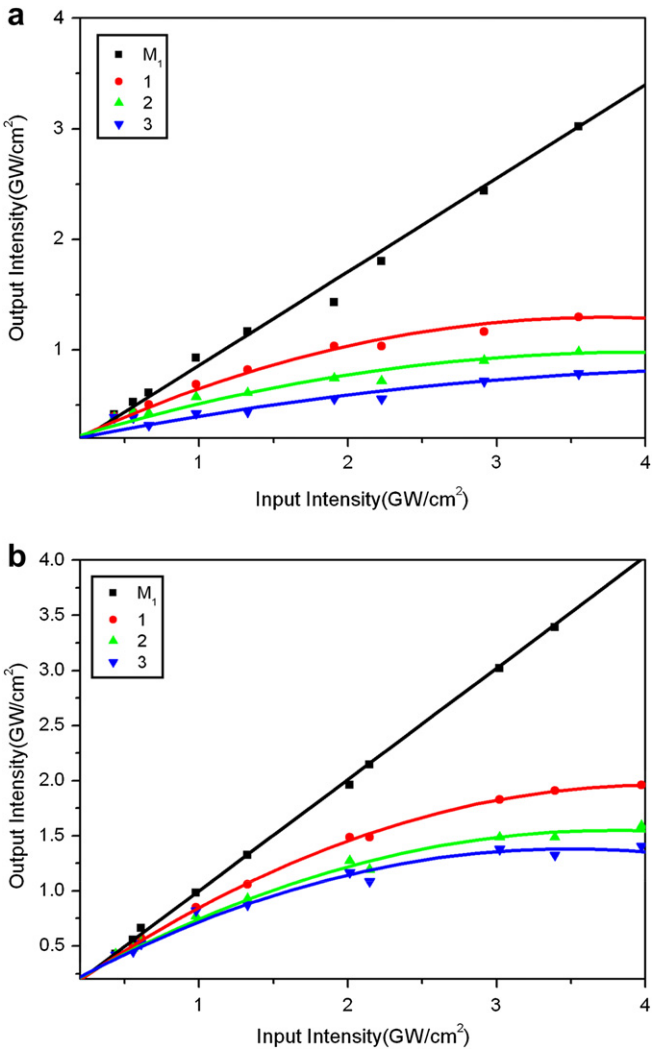

Fig. 8. Nonlinear transmission of chromophores **1**–**3** in CH_2Cl_2 (a) and DMF (b). From top downwards is M_1, **1**, **2**, **3**.

Table 3
Two-photon absorption properties of chromophores **1**–**3**

No.	λ_{TPEF} (nm)/CH_2Cl_2	β (cm/GW)	λ_{TPEF} (nm)/DMF	β (cm/GW)
1	502	2.8	516	1.1
2	515	4.9	523	1.9
3	518	8.9	494	2.9

$(\mu_{ee}-\mu_{gg})^2$, it is reasonable to suppose that these two quantities behave similarly. This empirical trend indicates that the degree of solvatochromism could provide a valuable tool for the estimation of the TPA magnitude.

Optical power limiting is an area of growing interest owing to applications such as eye and photodetector protection against intense tunable laser pulses. An ideal optical limiter is perfectly transparent at low intensities below a predetermined critical intensity level, above which the transmitted intensity remains at a constant value. The principle of optical power limiting effects is based on the fact that a large input signal change will only lead to a small output change. Fig. 8 shows the optical power limiting behavior of chromophores **1**–**3** measured by the NLT method. The basic parameters of this dye laser output are 800 nm wavelength, 8 ns pulse width, and 1–2 mJ pulse energy. In Fig. 8, one can easily find that at a high input level, a larger input intensity variation will result in much smaller output intensity variation due to the intrinsic TPA property. The most interesting feature of Fig. 8 is that the output/input curve levels off when the input intensity increases from $\sim$0.5 GW/cm^2 to $\sim$3.5 GW/cm^2. This type of output/input characteristic curve can be used for optical peak power limiting and stabilization, which means that a larger input peak power fluctuation will become a much smaller output fluctuation after passing through the nonlinear absorptive chromophores with a large TPA value. The optical limiting ability is in the order of chromophore **3** > chromophore **2** > chromophore **1** > M_1.

4. Conclusion

Three novel multipolar chromophores, *N*-{{{3,5-di-[5-(4-*tert*-butylphenyl)-1,3,4-oxadiazole-2]-phenyl}-vinyl}-4-phenyl}-diphenylamine, *N*,*N*-di{{{3,5-di-[5-(4-*tert*-butylphenyl)-1,3,4-oxadiazole-2]-phenyl}-vinyl}-4-phenyl}-phenylamine and *N*,*N*,*N*-tris{4-{2-{3,5-di-[5-(4-*tert*-butylphenyl)-1,3,4-oxadiazole-2]-phenyl}-1-vinyl}-phenyl}-amine, have been designed and synthesized through the Wittig and Heck reaction. Their structures were characterized by IR, ^{1}H NMR and MS, the UV and fluorescence spectra were obtained in different solvents. The relationship of Stokes shift and solvent polarity is discussed from the Lippert–Mataga equation. The branching effect on linear and nonlinear optical properties of multipolar structures has been studied. A number of factors influence the TPA magnitude, among which are electronic delocalization and intramolecular charge-transfer phenomena. This enhancement in TPA is correlated to an intramolecular charge redistribution that occurs between the ends and the center of the molecules. A very effective intramolecular charge transfer from the excited terminal units to the central core make the dominant contribution to the two-photon absorption. In the case of branched systems, inter-branch coherent coupling between the arms plays a major role.

Acknowledgements

The authors are grateful to the National Science Foundation of China No. 60678042, and the Natural Science Foundation of Southeast University No. 9207041399 and the Natural Science Foundation of Jiangsu Province of China No. BK2006553 for financial support.

References

[1] Bhaskar A, Guda R, Haley MM, Goodson TG. Building symmetric two-dimensional two-photon materials. J Am Chem Soc 2006;128(43):13972–3.
[2] Kannan R, He GS, Lin TC, Prasad PN, Vaia RA, Tan LS. Toward highly active two-photon absorbing liquids. Synthesis and characterization of octupolar molecules. Chem Mater 2004;16(1):185–94.
[3] Brousmiche DW, Serin JM, Frechet JMJ, He GS, Lin TC, Chung SJ, et al. Fluorescence resonance energy transfer in novel multiphoton absorbing dendritic structure. J Phys Chem B 2004;108(25):8592–600.
[4] Bhaskar A, Ramakrishna G, Lu Z, Twieg R, Hales JM, Hagan DJ, et al. Investigation of two-photon absorption properties in branched alkene and alkyne chromophores. J Am Chem Soc 2006;128(36):11840–9.
[5] Samoc M, Morrall JP, Dalton GT, Cifuentes MP, Humphrey MG. Two-photon and three-photon absorption in an organometallic dendrimer. Angew Chem Int Ed 2007;46:731–3.
[6] Drobrizhev M, Karotki A, Dzenis Y, Rebane A, Suo Z, Spangler CW. Strong cooperative enhancement of two-photon absorption in dendrimers. J Phys Chem B 2003;107(31):7540–3.
[7] Chung SJ, Kim KS, Lin TC, He GS, Swiatkiewicz J, Prasad PN. Cooperative enhancement of two-photon absorption in multi-branched structure. J Phys Chem B 1999;103(49):10741–5.
[8] Zheng Q, He GS, Prasad PN. π-Conjugated dendritic nanosized chromophore with enhanced two-photon absorption. Chem Mater 2005;17(24):6004–11.
[9] Li B, Tong R, Zhu R, Meng FS, Tian H, Qian SX. The ultrafast dyanamics and nonlinear optical properties of tribranched styryl derivatives based on 1,3,5-triazine. J Phys Chem B 2005;109:10705–10.
[10] Li J, Meng FS, Tian H, Mi J, Ji W. Highly fluorescent naphthalimide derivatives for two-photon absorption materials. Chem Lett 2005;34(7):922–3.
[11] Hua JL, Li B, Meng FS, Ding F, Qian SX, Tian H. Two-photon absorption properties of hyperbranched conjugated polymers with triphenylamine as the core. Polymer 2004;45:7143–9.
[12] Mallegol T, Gmouh S, Meziane MAM, Blanchard-Desce M, Mongin O. Practical and efficient synthesis of tris(4-formylphenyl)amine, a key building block in materials chemistry. Synthesis 2005;11:1771–4.
[13] Paul GK, Mwaura J, Argun AA, Taranekar P, Reynolds JR. Cross-linked hyperbranched arylamine polymers as hole-transporting materials for polymer LEDs. Macromolecules 2006;39(23):7789–92.
[14] Lee HJ, Sohn J, Hwang J, Park SY, Choi H, Cha M. Triphenylamine-cored bifunctional organic molecules for two-photon absorption and photorefraction. Chem Mater 2004;16(3):456–65.
[15] He GS, Lin T, Cui Y, Prasad PN, Brousmiche DW, Serin JM, et al. Two-photon excited intramolecular energy transfer and light-harvesting effect in novel dendritic systems. Opt Lett 2003;28(10):768–70.
[16] Terenziani F, Droumaguet CL, Katan C, Mongin O, Blanchard-Desce M. Effect of branching on two-photon absorption in triphenylbenzene derivatives. ChemPhysChem 2007;8:723–34.
[17] Katan C, Terenziani F, Mongin O, Wertz MHV, Porres L, Pons T, et al. Effects of multibranching of dipolar chromophores on photophysical properties and two-photon absorption. J Phys Chem A 2005;109(13):3024–37.
[18] He GS, Xu GC, Prasad PN, Reinhardt BA, Bhatt JC, Dillard AG. Two-photon absorption and optical-limiting properties of novel organic compounds. Opt Lett 1995;20(5):435–7.